period. Grafted RFP$^+$ cells were located mainly around the lesion epicenter, whereas some cells had migrated as far as 4 mm rostral and caudal to the graft site (Fig. 2*C*). In the injured spinal cord, the grafted 38C2 iPS-SNSs differentiated into three types of neural cells, including Hu$^+$ neurons (31.4 ± 1.1%), GFAP$^+$ astrocytes (49.3 ± 4.5%), and π-GST$^+$ oligodendrocytes (14.4 ± 3.0%), whereas 38C2 iPS-PNSs differentiated dominantly into neurons—that is, Hu$^+$ neurons (50.4 ± 3.8%), GFAP$^+$ astrocytes (14.9 ± 0.6%), and π-GST$^+$ oligodendrocytes (4.6 ± 1.8%) (Fig. 2 *D* and *E* and Fig. S6).

Transplantation of SNSs Derived from Safe MEF-iPS Cells into the Injured Spinal Cord Promotes Functional Recovery. The contusive SCI initially caused complete paralysis, followed by gradual recovery that reached a plateau. There were statistically significant differences in Basso mouse scale (BMS) between the 38C2 iPS-SNS and PBS groups at 21, 28, 35, and 42 d after injury, whereas no significant difference was observed between the 38C2 iPS-SNS and EB3 ES-SNS groups. Forty-two days after injury, the 38C2 iPS-SNS–grafted animals could lift their trunks and had significantly better BMS than the PBS control or adult fibroblast-treated animals, which were unable to support their body weight with their hindlimbs (Fig. 3*A*). To reveal the potential mechanism of functional recovery after 38C2 iPS-SNS transplantation, we conducted further histological analyses. By Luxol Fast Blue (LFB) staining, 38C2 iPS-SNS–grafted mice showed a significantly larger myelinated area at the lesion epicenter than the PBS control mice at 42 d after injury (Fig. 3*B*). We also found that grafted 38C2 iPS-SNS–derived cells myelinated NF200$^+$ host neuronal fibers, confirmed by the positive staining of RFP and myelin basic protein (MBP; Fig. 3*C*), indicating that graft cell-derived oligodendrocytes were capable of remyelination. For further confirmation of the myelinating ability of 38C2 iPS-SNSs, we transplanted 38C2 iPS-SNSs into the injured spinal cord of MBP-null *shiverer* mice, a severely hypo- and dysmyelinating mutant mouse that lacks the major dense line of CNS myelin (35). Myelinating potential of the grafted 38C2 iPS-SNS–derived cells was confirmed, exhibiting MBP$^+$ deposits (Fig. 3*D*) and the major dense line, by electron microscopic analysis (Fig. 3*E*).

To determine the effect of the grafted 38C2 iPS-SNSs on serotonergic nerve fibers, which are important for the motor functional recovery of hind limbs (36, 37), we immunostained for 5HT and quantified the positive area at the distal cord 1, 2, and 6 wk after injury. Some of the nerve fibers associated with graft cell-derived Hu$^+$ neurons were identified as 5HT$^+$ serotonergic fibers, and were prominent at the distal cord compared with the PBS control group (Fig. 4 *A*–*C*). Quantitative analysis of the serotonergic innervation of the distal cord revealed a significant difference between the 38C2 iPS-SNS and PBS control groups (Fig. 4*B*). The contusive injury (60 kDyn) resulted in a significant decrease in the number of 5HT$^+$ fibers at the distal cord, followed by a slight recovery, which is the nature of contusive SCI. The injection of PBS in the PBS control group did not induce any additional increase in the number of 5HT$^+$ fibers at the distal cord. In contrast, innervation of the distal cord by these 5HT$^+$ fibers was enhanced by the grafted 38C2 iPS-SNS 6 wk after SCI (Fig. 4*B*). Moreover, 38C2 iPS-SNS–derived astrocytes, which exhibited a bipolar morphology with long processes, were observed closely associated with the 5HT$^+$ serotonergic fibers (Fig. 4*D*).

Transplantation of Neurospheres Derived from Pre-Evaluated Safe or Unsafe TTF-iPS Cells into the Injured Spinal Cord. Toward the goal of clinical application, we next examined the therapeutic potential

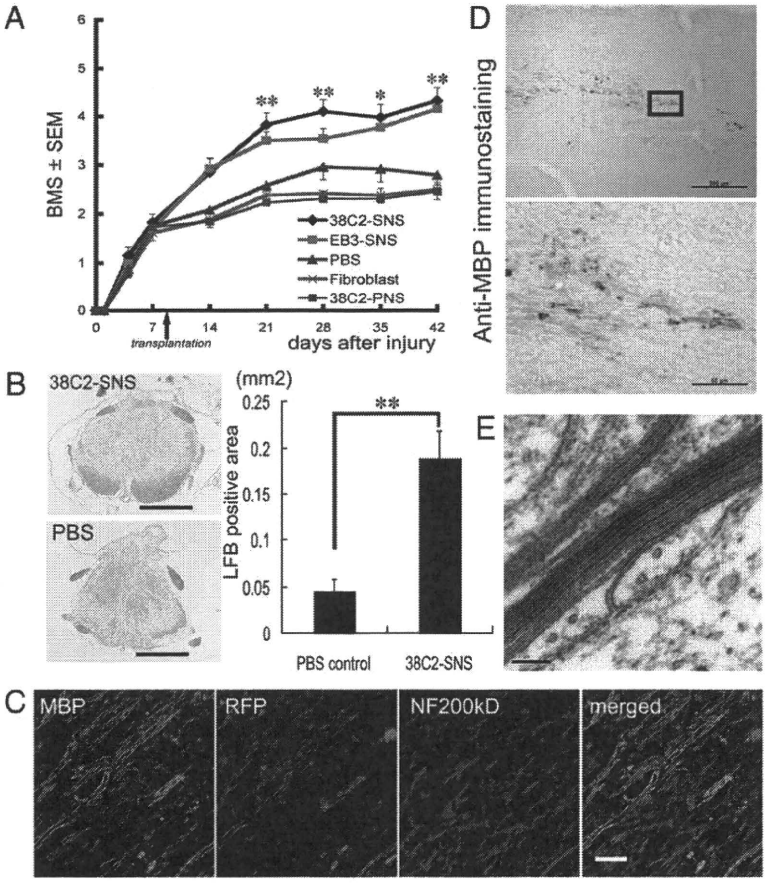

Fig. 3. SNS derived from a safe MEF-iPS clone differentiate into mature oligodendrocytes and promote remyelination. (*A*) Time course of functional recovery of hind limbs evaluated by BMS. 38C2 iPS-SNS, $n = 19$; EB3 ES-SNS, $n = 15$; PBS, $n = 12$; adult fibroblasts, $n = 13$; 38C2 iPS-PNS, $n = 13$. $^*P < 0.05$, $^{**}P < 0.01$. (*B*) LFB staining of axial sections of the spinal cord at the lesion epicenter 42 d after injury; 38C2 iPS-SNS–transplanted (*Upper Left*) and PBS control (*Lower Left*) animals. Quantification of LFB-positive areas at the lesion epicenter 42 d after injury (*Right*, $n = 7$ each; $^{**}P < 0.01$). (*C*) Immunohistochemistry of 38C2 iPS-SNS–derived mature oligodendrocytes (MBP$^+$). Grafted cells were integrated into myelin sheath. (*D*) Anti-MBP DAB staining of sagittally sectioned spinal cord of a *shiverer* mouse 8 wk after transplantation. MBP$^+$ myelin was detected in the area caudal to the lesion epicenter. (*Lower*) Higher-magnification image of the boxed area. (*E*) EM pictures of the injured spinal cord of a 38C2 iPS-SNS–grafted *shiverer* mouse exhibiting a prominent major dense line and intraperiod lines in multiple compacted lamellae. (Scale bars: *B*, 500 μm; *D Upper*, 200 μm; *C* and *D Lower*, 50 μm; and *E*, 0.1 μm.)

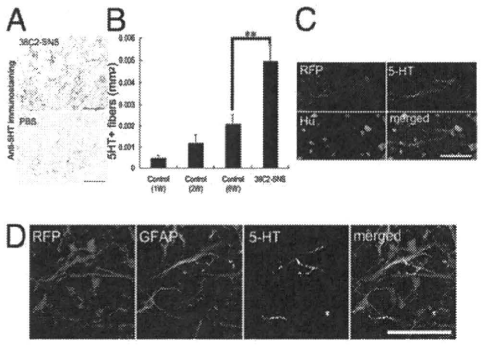

Fig. 4. SNSs derived from a safe MEF-iPS clone promote serotonergic innervation of the dorsal cord and result in better functional recovery of the hindlimbs. (*A*) 38C2 iPS-SNS transplantation promoted the growth of 5HT$^+$ serotonergic fibers in the distal spinal cord. Axial sections of 38C2 iPS-SNS–transplanted (*Upper*) and PBS control mice (*Lower*). (*B*) Quantitative analysis of 5HT$^+$ serotonergic fibers of distal cord in the PBS control (1, 2, and 6 wk postinjury) and 38C2 iPS-SNS transplantation groups (6 wk postinjury; 1 and 2 wk postinjury, $n = 3$ each; 6 wk postinjury and 38C2 SNS, $n = 7$ each; $^{**}P < 0.01$). (*C* and *D*) Immunohistochemistry of 38C2 iPS-SNS–derived neurons (*C*, RFP$^+$, Hu$^+$) and astrocytes (*D*, RFP$^+$, GFAP$^+$) closely associated with 5HT$^+$ serotonergic fibers. (Scale bars: *A*, 100 μm; *C*, 20 μm; *D*, 50 μm.)

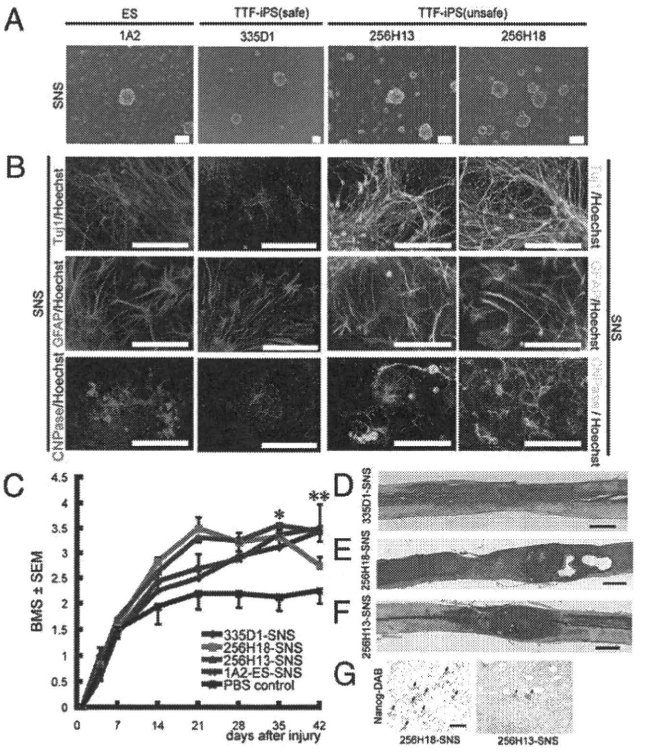

Fig. 5. Characterization and transplantation of SNSs derived from safe and unsafe TTF-iPS cells. (*A*) Neurospheres derived from 1A2 ES cells, 335D1, 256H13, and 256H18 iPS cells. (Scale bar: 200 μm.) (*B*) The differentiation potential of TTF-iPS-derived SNSs tested in vitro by immunocytochemical analyses of neural cell markers; Tuj1 for neurons, GFAP for astrocytes, and CNPase for oligodendrocytes. (Scale bar: 100 μm.) (*C*) Time course of functional recovery of the hindlimbs evaluated by BMS. 335D1 iPS-SNS: $n = 9$ each; 256H13 and 256H18 iPS-SNS: $n = 9$; 1A2 ES-SNS: $n = 9$; PBS control: $n = 8$. $^*P < 0.05$, $^{**}P < 0.01$. (*D–F*) H&E sagittal sections of the spinal cord 42 d after injury. (*D*) 335D1 iPS-SNS, (*E*) 256H18 iPS-SNS, and (*F*) 256H13 iPS-SNS grafted mice. There was no evidence of tumorigenesis in the 335D1 iPS-SNS grafted mice (*D*), whereas teratoma formation was detected within the injured spinal cord in both 256H18 iPS-SNS (*E*), and 256H13 iPS-SNS (*F*) grafted mice. (*G*) Anti-Nanog DAB staining of sagittally sectioned spinal cord of 256H18 and 256H13 iPS-SNS–transplanted animals 35 d after transplantation.

of adult tissue-derived iPS cells. Among six TTF-iPS clones pre-evaluated in our previous study (27), we used the safe 335D1 TTF-iPS clone, which was generated with *Nanog* selection and without the transduction of c-Myc. We also used the unsafe 256H13 and 256H18 TTF-iPS clones (22, 27), which were generated without genetic selection or the transduction of c-Myc, and were originally established from CAG-EGFP mice (22). A subclone of RF8 ES cells carrying the *Nanog*-EGFP reporter (1A2) (19) was used as control. All of the TTF-iPS clones formed PNSs and SNSs (Fig. 5*A*), and generated cells of all three neural lineages, similar to those derived from 1A2 ES cells (Fig. 5*B*). We transplanted these TTF-iPS–derived SNSs into injured spinal cords 9 d after injury. Transplantation of the safe 335D1 iPS-SNS (prelabeled with RFP lentivirally) resulted in better functional recovery compared with the PBS control group, without any apparent tumorigenesis during our observation period (Fig. 5 *C* and *D*). Grafted and survived RFP$^+$ 335D1 iPS-SNS–derived cells could differentiate into neural trilineages (Fig. S7 *A* and *B*). Furthermore, LFB staining revealed that 335D1 iPS-SNS–grafted mice had a significantly larger myelinated area at the lesion epicenter than the PBS control mice at 42 d after injury (Fig. S8 *A* and *B*), and grafted RFP$^+$ 335D1 SNS-derived cells differentiated into MBP$^+$ oligodendrocytes (Fig. S8*C*). However, all unsafe 256H18 iPS-SNS–grafted mice and one of 256H13 iPS-SNS–grafted mice formed teratomas containing EGFP$^+$ donor cells within the injured spinal cord (Fig. 5 *E* and *F* and Fig. S7*C*). Histological analyses revealed that these teratomas contained epithelial and smooth muscle tissue (Fig. S9*A*), and also exhibited Nanog immunoreactivity (Fig. 5*G*). Although the motor functions gradually recovered in both groups to the same extent as in the safe 335D1 iPS-SNS recipients until 35 d after injury, the 256H18 iPS-SNS–grafted animals exhibited a sudden deterioration of motor function 42 d after injury. In contrast, the 256H13 iPS-SNS–grafted animals maintained their functional recovery at 42 d after injury (Fig. 5*C*). Notably, in most mice of the 256H13 iPS-SNS group, scattered small clusters of Nanog$^+$ cells were observed in the spinal cords without obvious teratoma formation (Fig. S9 *B* and *C*). Thus, we speculate that teratoma formation and subsequent deterioration of function recovery would occur in the 256H13 group if a longer observation period was set.

Discussion

In the present study, we showed that the pre-evaluated safe iPS cells could produce neurospheres containing NS/PCs (Fig. 1*A*) that give rise to trilineage neural cells, including several types of neurons (Fig. 1 *B* and *C*), and that the neurons were electrophysiologically functional in vitro similar to ES cells (Fig. S2).

Based on these safety assessments and in vitro findings, we performed an in vivo study using the safe 38C2 MEF-iPS cell clone. Grafted 38C2 iPS-SNSs differentiated into neurons, astrocytes, and oligodendrocytes without forming teratomas or other tumors, and promoted functional recovery after SCI, whereas 38C2 iPS-PNSs did not show any therapeutic effects (Fig. 3*A*). These findings were compatible with our recent data on mouse ES cell-derived neurosphere transplantation into an identical mouse SCI model (31). Transplantation of ES-derived SNSs, which can differentiate into neural trilineages, promoted remyelination, axonal regrowth and tissue sparing, leading to improved function. In contrast, predominantly neurogenic PNSs showed no therapeutic effects on SCI (31). Thus, we elected to use iPS-SNSs and not iPS-PNSs for this study. In fact, the grafted 38C2 iPS-SNSs formed MBP$^+$ myelin sheaths within the injured spinal cord. We also confirmed the myelination potential of 38C2 iPS-SNS–derived cells in the spinal cord of the MBP-null *shiverer* mouse by electron microscopy (Fig. 3

D and *E*). These findings suggested the possibility of the remyelination of demyelinated axons by the grafted 38C2 iPS-SNS–derived oligodendrocytes, which may have contributed to the functional recovery of the grafted animals.

Another potential mechanism for functional recovery is axonal regrowth supported by iPS-SNS–derived astrocytes. Here, we observed grafted 38C2 iPS-SNS–derived $GFAP^+$ astrocytes, which exhibited a bipolar morphology with long processes extending along the axis of the spinal cord, caudal to the lesion epicenter, in close association with $5HT^+$ host serotonergic fibers (Fig. 4*D*). A previous report indicated that immature astrocytes derived from cells grafted into the injured spinal cord promote the outgrowth of $5HT^+$ fibers by offering a growth-permissive surface (38). Consistent with this finding, the transplantation of 38C2 iPS-SNSs promoted serotonergic innervation of the distal cord compared with the PBS control animals, thereby enhancing functional recovery after SCI (Fig. 4 *A* and *B*) (36). Furthermore, trophic factors, such as neurotrophin-3 (NT-3) and brain-derived neurotrophic factor (BDNF), were expressed in 38C2 iPS-SNSs, which could act as an integral part of the observed functional recovery (39, 40). The tissue sparing (e.g., neuroprotection, axon sprouting and remyelination) and other effects, including functional remodeling of spinal locomotor circuits (41), of trophic factors secreted from grafted cells are considered to be important for functional recovery (42). Thus, the combined effects of the 38C2 iPS-SNS–derived glial cells probably contributed to locomotor function recovery.

For clinical applications, the findings with TTF-iPS cells were promising, as most SCI patients are adults. The transplantation of SNSs derived from a pre-evaluated safe TTF-iPS clone promoted functional recovery after SCI without teratoma formation, like the SNSs from safe MEF-iPS clone did (Fig. 5*D*). However, the transplantation of SNSs derived from the unsafe TTF-iPS cells resulted in teratoma formation and functional deterioration. The teratoma-forming activity of TTF-iPS-SNSs could be caused by the presence of undifferentiated cells that might be resistant to differentiation signals within the SNSs (27). In fact, we recently reported that persistent presence of undifferentiated cells within iPS-SNSs highly correlated with teratoma-forming propensity, assayed by flow cytometric analysis using *Nanog*-EGFP reporter and transplantation into the brains of immunodeficient (NOD/SCID) (27). Before iPS cells of adult origin can be used clinically, important hurdles must still be overcome. Though new methods for establishing iPS cells are constantly being developed, including virus-free (43) and transgene-free (44) systems, a new strategy is needed to exclude undifferentiated cells from the differentiated progeny of iPS cells. These findings show that the pre-evaluation of iPS cells' in vitro differentiation potential could play a critical role in terms of their safety and therapeutic effects on the mouse SCI model. Thus, iPS-derived neurosphere transplantation has potential therapeutic use in SCI, when the iPS cell clones are carefully pre-evaluated.

From a clinical viewpoint, it is particularly encouraging that delaying the iPS-derived NS/PC transplantation (to 9 d after injury) enhanced both the survival of the grafted cells and functional recovery, the therapeutic effects of which is almost comparable to those of fetal CNS-derived NS/PCs transplantation (refs. 34 and 45). This finding may also be applicable to the treatment of patients with SCI. Since our first report of iPS cells (18), there has been increasing interest in their characteristics and therapeutic potential. Our present study demonstrates the therapeutic potential of iPS-derived NS/PCs for SCI repair. Before any clinical trial of human CNS disorders using iPS cells, it will be essential to pre-evaluate each iPS cell clone carefully to guarantee a safety level equal to other types of cells, such as Schwann cells (46, 47) and fetal-derived neurosphere cells (NS/PCs) (3), and to conduct preclinical transplantation studies using appropriate primate models (48, 49).

Methods

Reverse-Transcription and RT-PCR. RNA was isolated with TRIzol (Invitrogen) according to the manufacturer's instructions. Total RNA (0.5 μg) was treated with TURBO DNase (Ambion) and then reverse-transcribed with oligo (dT) primer and SuperScript III (Invitrogen). The primers and PCR conditions used in this study are listed Table S1.

Cell Culture, Neural Induction, and Immunocytochemistry. Mouse ES and iPS cells were cultured as described previously (19, 28, 29). Mouse ES and iPS cells were differentiated into neurospheres via EBs treated with 10^{-8} M retinoic acid (Sigma), as described previously with minor modification (28, 29). (Detailed differentiation protocol is described in *SI Text*.) ES and iPS cell-derived neurospheres were dissociated and differentiated on poly-L-ornithine/fibronectin-coated coverslips for 5 d and subjected to immunocytochemical analysis. The number of cells immunoreactive for each marker was counted and shown as the percentage of the total number of cells counterstained with Hoechst 33258. The antibodies used in this study are listed in Table S2.

Lentivirus Production and Infection of Secondary Neurospheres. For BLI tracing of grafted 38C2 iPS-SNSs, we generated a modified lentivirus vector encoding both the click beetle red luciferase (CBR/*uc*; Promega) and mRFP, pCSII-EF-CBR/*uc*-IRES2-mRFP (32, 33). For lentivirus preparation, HEK-293T cells were transfected with pCSII-EF-CBR/*uc*-IRES2-mRFP, pCAG-HIVgp, and pCMV-VSV-G-RSV-Rev, and the conditioned medium containing virus particles was concentrated and used for viral transduction.

Spinal Cord Injury Model and Transplantation. Adult female C57BL/6J mice (20–22 g) were anesthetized via an i.p. injection of ketamine (100 mg/kg) and xylazine (10 mg/kg). A contusive spinal cord injury using an Infinite Horizon Impactor (60 kdyn; Precision Systems) was induced at the Th10 level as reported previously (34). For transplantation, 5×10^5 cells of mouse ES/iPS cell-derived neurospheres, adult dermal fibroblasts in 2 μL of cell suspension, or PBS was injected into the lesion epicenter. Hindlimb motor function was evaluated by the locomotor rating of the Basso mouse scale (BMS) (50) for 42 d after injury. For the in vivo imaging of intact and injured spinal cords after the transplantation, a Xenogen-IVIS 100 cooled CCD optical macroscopic imaging system (SC BioScience) was used for BLI, as reported previously (34) (*SI Text*). All procedures were approved by the ethics committee of Keio University, and were in accordance with the Guide for the Care and Use of Laboratory Animals (National Institutes of Health). Grafted animals were deeply anesthetized and intracardially perfused with 4% paraformaldehyde (PFA; pH 7.4). The dissected spinal cords were sectioned into 20-μm axial/sagittal sections using a cryostat and processed for histological analyses. Detailed conditions for histological analyses are described in *SI Text*.

Statistical Analysis. All data are reported as the mean ± SEM. An unpaired two-tailed Student's *t* test was used for the analyses of in vitro and in vivo 38C2 iPS-SNS and ES-SNS differentiation efficiency (Figs. 1*C* and 2*E*), $5HT^+$ areas (Fig. 4*B*), and LFB^+ areas (Fig. 2*B*). Repeated-measures two-way ANOVA, followed by the Tukey–Kramer test, was used for BMS analysis. $^*P < 0.05$, $^{**}P < 0.01$.

ACKNOWLEDGMENTS. We thank Drs. H. Abe, T. Sunabori, F. Renault-Mihara, W. Akamatsu, S. Shibata, T. Harada, S. Miyao, and H. J. Okano (Keio University) for technical assistance and scientific discussions, and all the members of Dr. Okano's and Dr. Yamanaka's laboratories for encouragement and generous support. We also thank Drs. K. Okita, M. Koyanagi, and K. Tanabe (Kyoto University) for the undifferentiated iPS cells, Dr. H. Niwa (Riken CDB) for the EB3 ES cells, Dr. R. Farese (University of California-San Francisco) for the RF8 ES cells, Dr. R. Y. Tsien (University of California-San Diego) for the mRFP gene, Dr. A. Miyawaki (Riken BSI) for the Venus gene, Dr. H. Baba (Tokyo University of Phamacy and Life Science) for the shiverer mice, and Dr. H. Miyoshi (Riken BRC) for the lentiviral vectors. We especially thank Drs. S. Okada (Kyusyu University), A. Iwanami (University of California-San Francisco and Keio University), and J. Yamane (Keio University) for scientific discussions, technical advice, and encouragement. This work was supported by grants from the Program for Promotion of Fundamental Studies in Health Sciences of the National Institute of Biomedical Innovation (NIBIO), a grant from Uehara Memorial Foundation, and Grants-in-Aid for Scientific Research from the Japan Society for the Promotion of Science (JSPS) and the Ministry of Education, Culture, Sports, Science and Technology of Japan (MEXT), the project for realization of regenerative medicine and support for the core institutes for iPS cell research from MEXT; Japan Science and Technology Agency (SORST); the Ministry of Health, Labor, and Welfare; the General Insurance Association of Japan; Research Fellowships for Young Scientists from the Japan Society for the Promotion of Science; Keio Gijuku Academic Development Funds; and a Grant-in-aid for the Global COE program from MEXT to Keio University.

1. Björklund A, Lindvall O (2000) Cell replacement therapies for central nervous system disorders. *Nat Neurosci* 3:537–544.
2. Okano H (2002) Stem cell biology of the central nervous system. *J Neurosci Res* 69: 698–707.
3. Lindvall O, Kokaia Z, Martinez-Serrano A (2004) Stem cell therapy for human neurodegenerative disorders—how to make it work. *Nat Med* 10 (Suppl):S42–S50.
4. Martino G, Pluchino S (2006) The therapeutic potential of neural stem cells. *Nat Rev Neurosci* 7:395–406.
5. Lindvall O, Kokaia Z (2006) Stem cells for the treatment of neurological disorders. *Nature* 441:1094–1096.
6. Gage FH (2000) Mammalian neural stem cells. *Science* 287:1433–1438.
7. Wichterle H, Lieberam I, Porter JA, Jessell TM (2002) Directed differentiation of embryonic stem cells into motor neurons. *Cell* 110:385–397.
8. Watanabe K, et al. (2005) Directed differentiation of telencephalic precursors from embryonic stem cells. *Nat Neurosci* 8:288–296.
9. Sonntag KC, et al. (2007) Enhanced yield of neuroepithelial precursors and midbrain-like dopaminergic neurons from human embryonic stem cells using the bone morphogenic protein antagonist noggin. *Stem Cells* 25:411–418.
10. Tropepe V, et al. (2001) Direct neural fate specification from embryonic stem cells: A primitive mammalian neural stem cell stage acquired through a default mechanism. *Neuron* 30:65–78.
11. Ying QL, Stavridis M, Griffiths D, Li M, Smith A (2003) Conversion of embryonic stem cells into neuroectodermal precursors in adherent monoculture. *Nat Biotechnol* 21: 183–186.
12. McDonald JW, et al. (1999) Transplanted embryonic stem cells survive, differentiate and promote recovery in injured rat spinal cord. *Nat Med* 5:1410–1412.
13. Brüstle O, et al. (1999) Embryonic stem cell-derived glial precursors: A source of myelinating transplants. *Science* 285:754–756.
14. Kim JH, et al. (2002) Dopamine neurons derived from embryonic stem cells function in an animal model of Parkinson's disease. *Nature* 418:50–56.
15. Sharp J, Keirstead HS (2007) Therapeutic applications of oligodendrocyte precursors derived from human embryonic stem cells. *Curr Opin Biotechnol* 18:434–440.
16. Keirstead HS, et al. (2005) Human embryonic stem cell-derived oligodendrocyte progenitor cell transplants remyelinate and restore locomotion after spinal cord injury. *J Neurosci* 25:4694–4705.
17. Hochedlinger K, Jaenisch R (2006) Nuclear reprogramming and pluripotency. *Nature* 441:1061–1067.
18. Takahashi K, Yamanaka S (2006) Induction of pluripotent stem cells from mouse embryonic and adult fibroblast cultures by defined factors. *Cell* 126:663–676.
19. Okita K, Ichisaka T, Yamanaka S (2007) Generation of germline-competent induced pluripotent stem cells. *Nature* 448:313–317.
20. Wernig M, et al. (2007) In vitro reprogramming of fibroblasts into a pluripotent ES-cell-like state. *Nature* 448:318–324.
21. Maherali N, et al. (2007) Directly reprogrammed fibroblasts show global epigenetic remodeling and widespread tissue contribution. *Cell Stem Cell* 1:55–70.
22. Nakagawa M, et al. (2008) Generation of induced pluripotent stem cells without Myc from mouse and human fibroblasts. *Nat Biotechnol* 26:101–106.
23. Wernig M, Meissner A, Cassady JP, Jaenisch R (2008) c-Myc is dispensable for direct reprogramming of mouse fibroblasts. *Cell Stem Cell* 2:10–12.
24. Hanna J, et al. (2007) Treatment of sickle cell anemia mouse model with iPS cells generated from autologous skin. *Science* 318:1920–1923.
25. Wernig M, et al. (2008) Neurons derived from reprogrammed fibroblasts functionally integrate into the fetal brain and improve symptoms of rats with Parkinson's disease. *Proc Natl Acad Sci USA* 105:5856–5861.
26. Yamanaka S (2007) Strategies and new developments in the generation of patient-specific pluripotent stem cells. *Cell Stem Cell* 1:39–49.
27. Miura K, et al. (2009) Variation in the safety of induced pluripotent stem cell lines. *Nat Biotechnol* 27:743–745.
28. Okada Y, et al. (2008) Spatiotemporal recapitulation of central nervous system development by murine embryonic stem cell-derived neural stem/progenitor cells. *Stem Cells* 26:3086–3098.
29. Okada Y, Shimazaki T, Sobue G, Okano H (2004) Retinoic-acid-concentration-dependent acquisition of neural cell identity during in vitro differentiation of mouse embryonic stem cells. *Dev Biol* 275:124–142.
30. Niwa H, Miyazaki J, Smith AG (2000) Quantitative expression of Oct-3/4 defines differentiation, dedifferentiation or self-renewal of ES cells. *Nat Genet* 24:372–376.
31. Kumagai G, et al. (2009) Roles of ES cell-derived gliogenic neural stem/progenitor cells in functional recovery after spinal cord injury. *PLoS ONE* 4:e7706.
32. Masuda H, et al. (2007) Noninvasive and real-time assessment of reconstructed functional human endometrium in NOD/SCID/gamma c(null) immunodeficient mice. *Proc Natl Acad Sci USA* 104:1925–1930.
33. Miyoshi H, Blömer U, Takahashi M, Gage FH, Verma IM (1998) Development of a self-inactivating lentivirus vector. *J Virol* 72:8150–8157.
34. Okada S, et al. (2005) In vivo imaging of engrafted neural stem cells: Its application in evaluating the optimal timing of transplantation for spinal cord injury. *FASEB J* 19: 1839–1841.
35. Inoue Y, et al. (1986) Alteration of the primary pattern of central myelin in a chimaeric environment—study of shiverer ↔ wild-type chimaeras. *Brain Res* 391:239–247.
36. Bregman BS, et al. (1993) Recovery of function after spinal cord injury: Mechanisms underlying transplant-mediated recovery of function differ after spinal cord injury in newborn and adult rats. *Exp Neurol* 123:3–16.
37. Nygren LG, Fuxe K, Jonsson G, Olson L (1974) Functional regeneration of 5-hydroxytryptamine nerve terminals in the rat spinal cord following 5, 6-dihydroxytryptamine induced degeneration. *Brain Res* 78:377–394.
38. Hofstetter CP, et al. (2002) Marrow stromal cells form guiding strands in the injured spinal cord and promote recovery. *Proc Natl Acad Sci USA* 99:2199–2204.
39. Widenfalk J, Lundströmer K, Jubran M, Brene S, Olson L (2001) Neurotrophic factors and receptors in the immature and adult spinal cord after mechanical injury or kainic acid. *J Neurosci* 21:3457–3475.
40. McTigue DM, Horner PJ, Stokes BT, Gage FH (1998) Neurotrophin-3 and brain-derived neurotrophic factor induce oligodendrocyte proliferation and myelination of regenerating axons in the contused adult rat spinal cord. *J Neurosci* 18:5354–5365.
41. Courtine G, et al. (2009) Transformation of nonfunctional spinal circuits into functional states after the loss of brain input. *Nat Neurosci* 12:1333–1342.
42. Lu P, Tuszynski MH (2008) Growth factors and combinatorial therapies for CNS regeneration. *Exp Neurol* 209:313–320.
43. Okita K, Nakagawa M, Hyenjong H, Ichisaka T, Yamanaka S (2008) Generation of mouse induced pluripotent stem cells without viral vectors. *Science* 322:949–953.
44. Zhou H, et al. (2009) Generation of induced pluripotent stem cells using recombinant proteins. *Cell Stem Cell* 4:381–384.
45. Ogawa Y, et al. (2002) Transplantation of in vitro-expanded fetal neural progenitor cells results in neurogenesis and functional recovery after spinal cord contusion injury in adult rats. *J Neurosci Res* 69:925–933.
46. Pearse DD, et al. (2004) cAMP and Schwann cells promote axonal growth and functional recovery after spinal cord injury. *Nat Med* 10:610–616.
47. Pearse DD, et al. (2007) Transplantation of Schwann cells and/or olfactory ensheathing glia into the contused spinal cord: Survival, migration, axon association, and functional recovery. *Glia* 55:976–1000.
48. Iwanami A, et al. (2005) Establishment of graded spinal cord injury model in a nonhuman primate: The common marmoset. *J Neurosci Res* 80:172–181.
49. Iwanami A, et al. (2005) Transplantation of human neural stem cells for spinal cord injury in primates. *J Neurosci Res* 80:182–190.
50. Basso DM, et al. (2006) Basso Mouse Scale for locomotion detects differences in recovery after spinal cord injury in five common mouse strains. *J Neurotrauma* 23:635–659.

Hindawi Publishing Corporation
Journal of Biomedicine and Biotechnology
Volume 2011, Article ID 157458, 7 pages
doi:10.1155/2011/157458

Research Article

Novel Concept of Motor Functional Analysis for Spinal Cord Injury in Adult Mice

Munehisa Shinozaki,[1,2] Yuichiro Takahashi,[3] Masahiko Mukaino,[4] Nobuhito Saito,[2] Yoshiaki Toyama,[3] Hideyuki Okano,[1] and Masaya Nakamura[3]

[1] *Department of Physiology, Keio University School of Medicine, Shinjuku, Tokyo 160-8582, Japan*
[2] *Department of Neurosurgery, Graduate School of Medicine, University of Tokyo, Tokyo 113-8655, Japan*
[3] *Department of Orthopedic Surgery, Keio University School of Medicine, Shinjuku, Tokyo 160-8582, Japan*
[4] *Department of Rehabilitation Medicine, Keio University School of Medicine, Shinjuku, Tokyo 160-8582, Japan*

Correspondence should be addressed to Masaya Nakamura, masa@sc.itc.keio.ac.jp

Received 9 September 2010; Accepted 2 December 2010

Academic Editor: Monica Fedele

In basic research on spinal cord injury (SCI), behavioral evaluation of the SCI animal model is critical. However, it is difficult to accurately evaluate function in the mouse SCI model due to the small size of mice. Although the open-field scoring scale is an outstanding appraisal method, supplementary objective tests are required. Using a compact SCANET system, in which a mouse carries out free movement for 5 min, we developed a novel method to detect locomotor ability. A SCANET system samples the horizontal coordinates of a mouse every 0.1 s, and both the speed and acceleration of its motion are calculated at each moment. It was found that the maximum speed and acceleration of motion over 5 min varied by injury severity. Moreover, these values were significantly correlated with open-field scores. The maximum speed and acceleration of SCI model mice using a SCANET system are objective, easy to obtain, and reproducible for evaluating locomotive function.

1. Introduction

In basic research on spinal cord injury (SCI), accurate evaluation of motor function in animal models is important. Although the Basso-Beattie-Bresnahan (BBB) score and the Basso Mouse Scale (BMS) are widely used [1, 2], objective supplemental tests are desirable, and various methods have been developed [3–8]. However, with any method of observing the motion of an animal, detection of the best performance of the hindlimbs is almost impossible, since the animal does not perform as the observer intends. A novel method to evaluate the maximum locomotor ability of a mouse using the SCANET system is presented [9]. SCANET system is originally a device which measures voluntary motor activity of an animal. It consists of 45-cm-square Plexiglas cage, frames which contain infrared sensors and enclose the cage, and a notebook computer. Infrared sensors were horizontally placed throughout the cage, and the X-Y coordinates of a freely moving animal in the box were recorded every 0.1 s. After recording for 5 min, the change in the coordinates per unit time was calculated for the speed, and the change in the speed per unit time was calculated as the acceleration. The maximum speed and maximum acceleration extracted from the 5 min of data were taken as the best locomotor function. There were significant differences in these parameters among the contusion, the transection, and the control groups throughout the observation period, and, especially in the contusion group, they were significantly correlated with the BMS score during the recovery process.

2. Materials and Methods

2.1. Spinal Cord Injury Model. Seventeen 6-week-old adult female C57BL/6J mice were used. The mice were anesthetized with an intraperitoneal injection of ketamine (100 mg/kg) and xylazine (10 mg/kg). The dorsal surface of the dura mater at the T10 level was exposed by laminectomy, and spinal cord injury was induced by (1) producing moderate

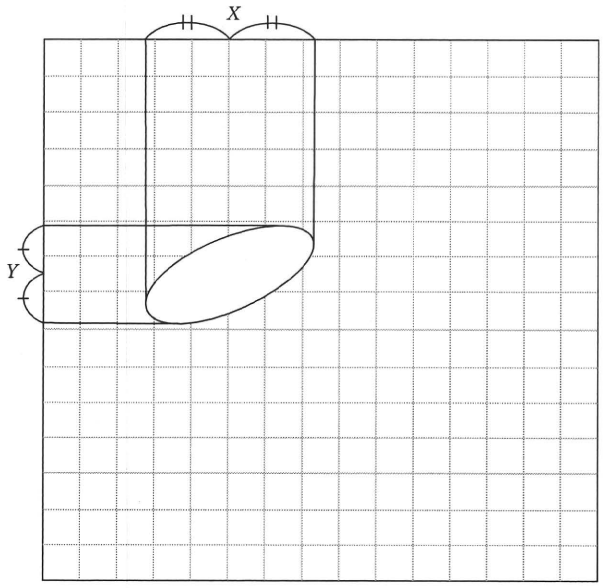

FIGURE 1: Schema of the inside of the Plexiglas cage. An ellipse expressed a mouse. Infrared sensors were arranged in a grid pattern, and the coordinates X and Y of the center of the object were recorded continuously.

contusion with an IH impactor ($n = 6$, impact force = 60 kdyn), as reported previously [10] or (2) transecting the spinal cord transversely with microscissors ($n = 6$). Only laminectomy was performed in the control group ($n = 5$). The muscles and skin were closed in layers, and the animals were placed in a temperature-controlled chamber until thermoregulation was re-established. Manual voiding of the bladder was performed twice per day until reflex bladder emptying was re-established. All the experiments and procedures in our study were approved by the Keio University Animal Research Committee in accordance with the Laboratory Animal Welfare Act, the Guide for the Care and Use of Laboratory Animals (National Institutes of Health, Bethesda, USA), and the Guidelines and Policies for Animal Surgery provided by the Animal Study Committees of the Central Institute for Experimental Animals and of Keio University.

2.2. Basso Mouse Scale Score. Motor function of the hindlimbs was evaluated by open-field testing using the methodology of the Basso Mouse Scale (BMS) score on postoperative days (POD) 1, 7, 14, 21, 28, 35, and 42, as described by Basso et al. [2].

2.3. SCANET. The SCANET MV-40 (MELQUEST Co., Ltd., Toyama, Japan) is an automatic analysis system for measuring the locomotor activity of small animals that has been previously described in [9, 11]. Briefly, infrared sensors are arranged in a horizontal plane of a transparent Plexiglas box of 45 cm around to make a sensor field with a 6-mm grid pattern. When something interferes with the paths of the infrared rays, the coordinates of the center of the object

TABLE 1: An example of the list of raw data, calculated speed, and acceleration.

Time (mm:ss.f)	X	Y	Speed (m/s)	Acceleration (m/s^2)
—	—	—	—	—
—	$X1$	$Y1$	—	—
—	$X2$	$Y2$	$S1$	—
59:09.6	3.5	8.5	$S2$	$A1$
59:09.7	4.0	9.0	0.0424	$A2$
59:09.8	4.0	7.0	0.1200	0.7757
59:09.9	5.0	5.5	0.1082	−0.1183
59:10.0	6.5	4.5	0.1082	0.0000
59:10.1	6.0	7.0	0.1530	0.4480
59:10.2	4.0	16.0	0.5532	4.0020
—	—	—	—	—

are recorded in a computer every 0.1 s (Figure 1). Moreover, by inserting another sensor frame perpendicularly, we can simultaneously observe at different height levels and detect rearing of the mouse. The height of the lower frame was set at 1.5 cm from the floor, and the upper frame was 9.5 cm from the floor. We waited for 10 s after putting each mouse into the box until it calmed down, and then we measured for 5 min. The test was conducted 1, 7, 14, 21, 35, and 42 days after injury in the same environment. The default data obtained by SCANET system are "M1," which is the number of episodes of movement longer than 12 mm "M2," which is the number of episodes of movement longer than 60 mm; "RG," which is the number of episodes of rearing. However, the X and Y coordinates are recorded as raw data every 0.1 s and are available from the computer (Table 1). From these, the amount of the distance moved per unit time (speed) and the change in the speed per unit time (acceleration) were calculated at each instant of time. Since the time interval was 0.1 s and the unit length in raw data was 0.6 cm, speed and acceleration were calculated as follows:

$$\text{Speed } (S1) = \left\{(X2 \times 0.006 - X1 \times 0.006)^2 + (Y2 \times 0.006 - Y1 \times 0.006)^2\right\}^{0.5} \times 10\,(\text{m/s}), \quad (1)$$

$$\text{Acceleration } (A1) = (S2 - S1) \times 10\,(\text{m/s}^2).$$

Then, the maximum speed and the maximum acceleration were extracted from the whole 5 min of data as measures of the best locomotor function. Since the SCANET system sometimes lacks the time or coordinate data for a moment, only successive data were used.

2.4. Histological Analysis. To confirm the reproducibility of SCI model in each mouse, histological analysis was performed. 56 days after SCI, all animals were deeply anesthetized with an intraperitoneal injection of ketamine (100 mg/kg) and xylazine (10 mg/kg) and transcardially perfused with 4% paraformaldehyde in 0.1 M phosphate-buffered saline (PBS). The spinal cord tissue was removed

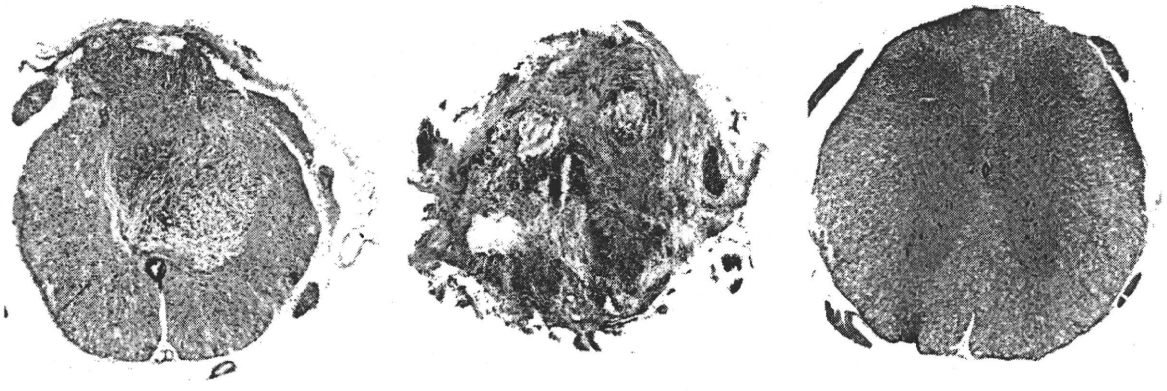

(a) (b) (c)

FIGURE 2: HE staining of representative axial spinal cord sections from the three groups of mice. (a) Contusion model: the ventral part of the spinal cord tissue was preserved, whereas the dorsal part was replaced by fibrous scar tissue after SCI. (b) Transection model: normal structure of the spinal cord totally disappeared. (c) Control mouse.

and postfixed in 4% paraformaldehyde in PBS for a few hours at room temperature. The tissue samples were immersed in 10% sucrose in PBS at 4°C for 24 hs, placed in 30% sucrose in PBS for 48 hs, and embedded in OTC compound. The embedded tissue was immediately frozen in liquid nitrogen and stored at −80°C until use. Frozen spinal cord tissues were sectioned on a cryostat at 20 μm in the axial plane. The sections were dried and stained with hematoxylin and eosin.

2.5. Statistics Analysis. All values are reported as the means ± SEM. Between-group comparisons were made by analysis of variance (ANOVA) followed by Scheffe's post hoc test at each postinjury time point. The strength of correlation with the BMS score was determined using the Pearson correlation coefficient.

3. Result

3.1. Histological Findings. The representative axial sections of the transection and contusion groups are shown in Figure 2. In the contusion group, infiltration of the inflammatory cells was observed at the dorsal part of the lesion site, and the ventral part of the spinal cord was preserved (Figure 2(a)). On the other hand, in the transection group, normal construction of the spinal cord was totally destroyed and replaced by inflammatory cells and fibrous tissues (Figure 2(b)).

3.2. BMS Score. Both the contusion and the transection injury resulted in complete paraplegia on POD 1 (Figure 3(a)). Although the BMS scores of the transection group did not show any recovery, those of the contusion group gradually increased and reached a plateau around a score of 4 on POD 14. Significant differences in BMS scores were observed among the three groups at all time points examined, except for POD 1.

3.3. Evaluation by SCANET. The control group showed the highest values of M1, M2, speed, and acceleration, followed by the contusion group and the transection group (Figure 3). The contusion and transection groups had very low RG numbers, while the control group had a stable number of RGs (Figure 3(d)). There were no significant differences in M1 and M2 among the three groups, except on PODs 1 and 21 (Figure 3(b)). However, speed was significantly different on PODs 14, 35, and 42 among the three groups, and the acceleration was significantly different on PODs 35 and 42 (Figures 3(e) and 3(f)). These results suggest that speed and acceleration reflected the severity of spinal cord injury better than M1 and M2 in the chronic phase of SCI.

3.4. Correlation between BMS Score and Speed/Acceleration of Movement. The correlation diagrams of M1, M2, speed, and acceleration with the BMS score in the contusion group are shown in Figure 4. Since M1 and M2 decreased gradually despite the increase in BMS score, there were no significant correlations between the BMS score and M1 and M2. On the other hand, speed and acceleration increased gradually, and the speed showed a significant correlation with the BMS score. These results suggest that the speed and acceleration are the best measures for observing functional recovery, not only to reflect the severity of injury.

3.5. Specific Features of Speed and Acceleration. For the BMS score, 5 min of observation are required for each mouse, so the same observation period was adopted for the present method. In order to examine how many minutes were suitable for the evaluation of the animal's performance by SCANET, the maximum speed of the mice on POD 42 was plotted for each time-duration (Figure 5). The maximum speed gradually increased and reached a plateau within 2 min in all groups. Therefore, 5 min were sufficient, and an even shorter examination time might has been enough for the SCANET evaluation.

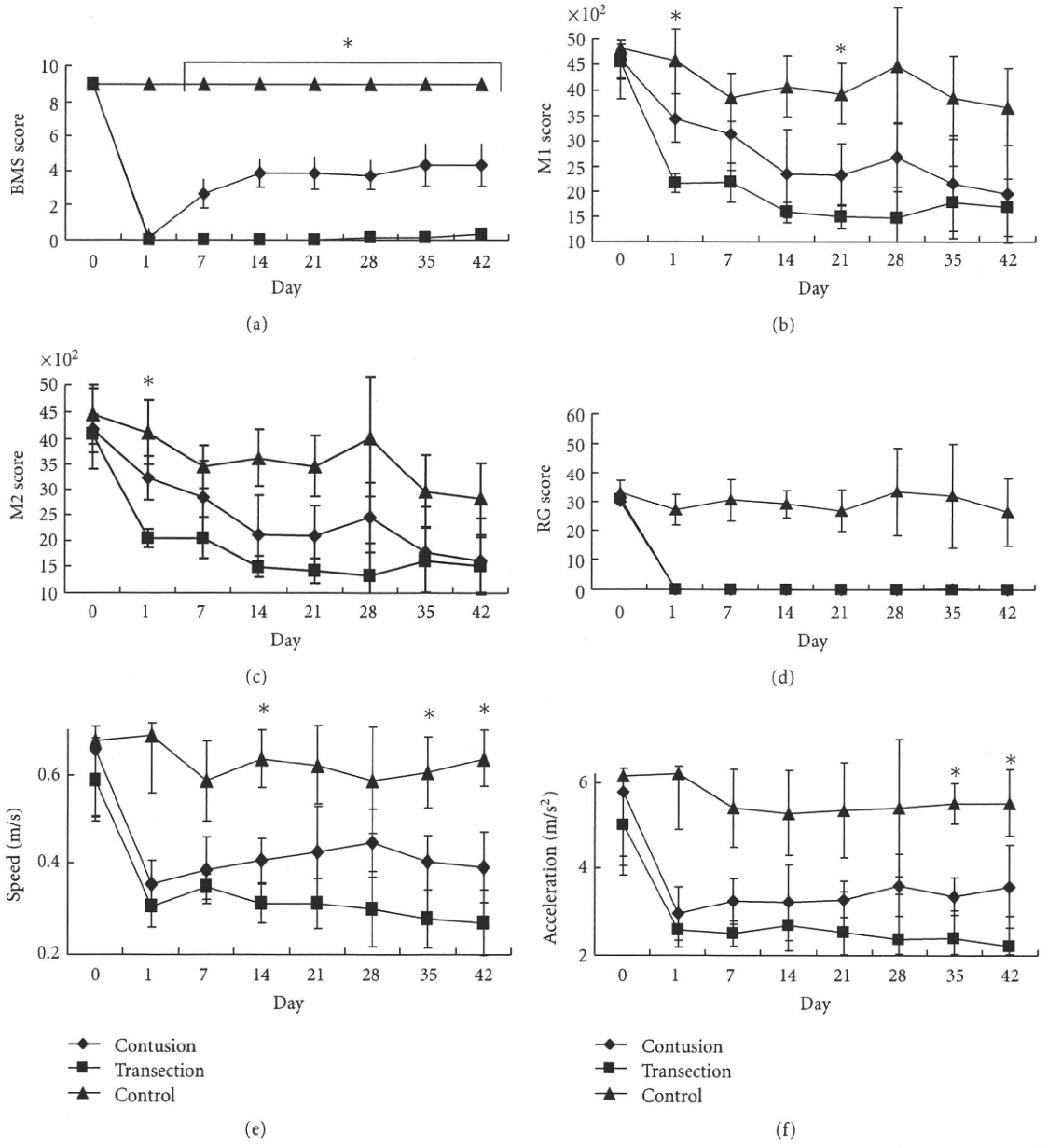

FIGURE 3: Time course of each parameter. (a) BMS score. (b) M1 score. (c) M2 score. (d) Rearing score (RG). (e) Speed. (f) Acceleration. M1 and M2 scores hardly showed a difference between the contusion and transection groups after 1 week, and they gradually decreased despite the animal's recovery of BMS score. The speed and acceleration showed clear differences among the three groups, especially in the late phase of SCI. $^*P < .05$.

The changes in speed and acceleration just before the maximum speed were also investigated, because we hypothesized that the mice with high BMS reached the maximum speed in a moment with their high instantaneous force, while the mice with low BMS increased their speed gradually. All mice reached the top speed within 0.1 s from a certain speed (Figure 6). The acceleration tended to decrease just before the maximum speed, and this might reflect the "premotion silent period" (exhaustion just before putting power into a voluntary muscle [12]) of an animal, because acceleration and muscle power were strongly correlated by the equation Force = Mass × Acceleration.

4. Discussion

In the present study, measurements of the maximum speed and acceleration of SCI model mice were found to be good indicators of the mice's motor performance, because they were constant in the control and transection groups and increased in the contusion group during the recovery of hindlimb function. In the transection group, the mice were not able to move their hindlimbs at all, but performed at half the speed of the control mice with only their forelimbs.

In this system, the moment of the best performance of a freely moving mouse can be detected. Therefore,

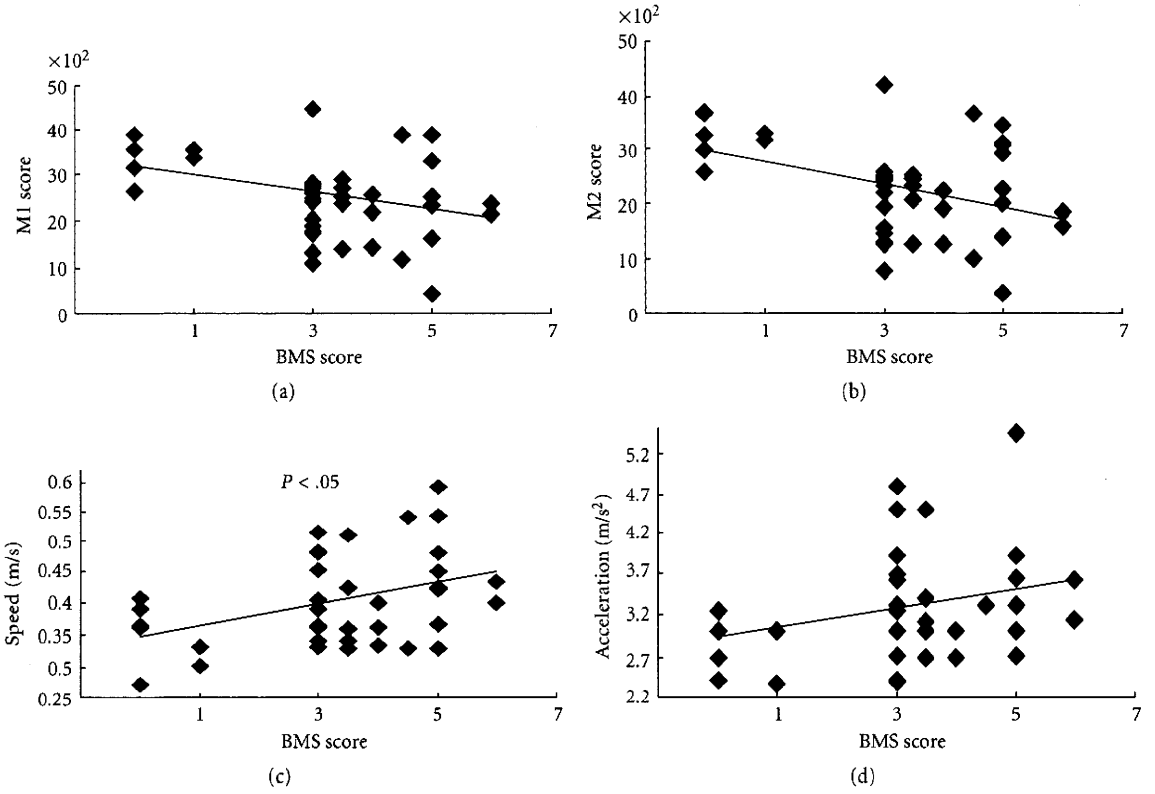

FIGURE 4: Correlation diagrams of parameters. M1 and M2 scores had minus correlations with the BMS score, while the speed and acceleration showed a strong correlation. Coefficients of correlation are −0.84 for M1 and BMS, −0.83 for M2 and BMS, 0.75 for speed and BMS, and 0.77 for acceleration and BMS.

the speed and acceleration may increase unwillingly if a mouse jumps by being surprised at a noise or a mouse is upset just after being put in the SCANET box. Avoidance of loud sound or shaking is critical for accurate evaluation.

Although the small movement M1 and the large movement M2 were also correlated with BMS at first, they gradually decreased during the follow-up period, as previously reported [9]. This might be due to the animal's habituation to the device, followed by lack of motivation. On the other hand, speed and acceleration did not decrease, suggesting that even a lackadaisical mouse had a moment to perform to its best ability during 5 min of observation. We also reconfirmed that the RG scores were almost zero in the contusion group, suggesting that it was difficult for C57BL/6 mice to stand up with only the hindlimbs after a 60-kdyn-contusive SCI.

Objectivity is one of the most important factors when evaluating motor function. While the open-field score is the simplest method, its value depends on the examiner, and subjectivity easily affects its accuracy [3]. Although evaluations using footprints or a treadmill seem objective, examiners discriminate certain parts or a range from the huge amount of data, so they still remain subjective [4, 5, 13]. In the present method, the values never vary by examiner and are calculated from the complete data, so they are always completely objective.

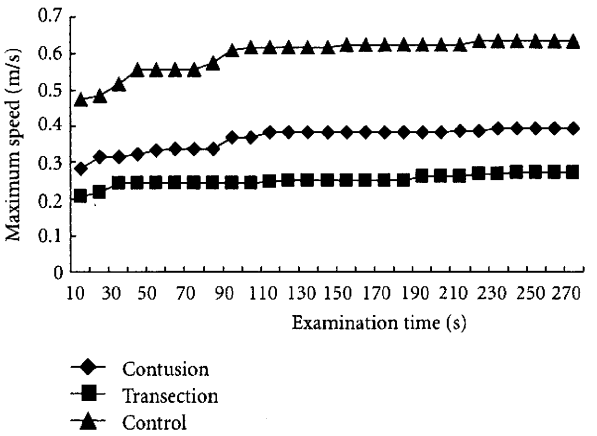

FIGURE 5: The maximum speed values to each time point were plotted with POD 42 data. They gradually increased and reached plateaus around 2 min in all groups. More than 2 minutes of examination time yielded slight difference.

Furthermore, ethical approval is necessary for animal studies, and the procedure must be as noninvasive as possible [14]. Behavioral analyses, such as the inclined test, beam walking test, and ladder test, cause mechanical stress to mice [7, 8, 15]. In belt-using devices, like a treadmill and automatic gait-recording machines, mouse behavior

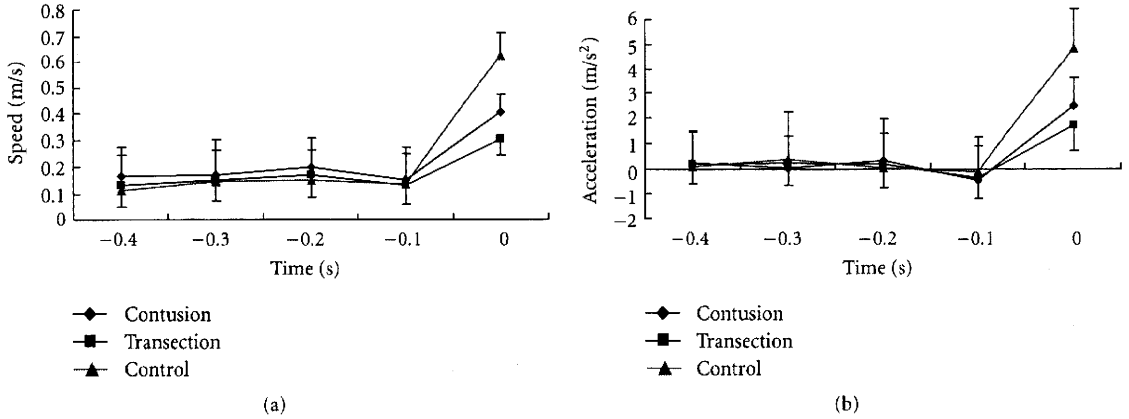

FIGURE 6: Shifting of the speed and acceleration just before reaching the maximum speed. Time 0 was the moment of maximum speed. Speed did not gradually increase to the maximum, and mice of all groups showed explosive power in 0.1 s to the maximum speed. Interestingly, acceleration 0.1 s before the maximum speed was under zero and that suggests muscles that were released just before strong contraction.

is severely restricted, and the moving belt sometimes harms the hindlimbs. With the present method, mice move freely as in a cage, and there is no stimulation and little stress. Hence, the present method is entirely noninvasive.

A simple and easy procedure is also desired for long-term follow-up of mice. Behavioral analysis, such as the inclined test, the beam walking test, or the ladder test, requires simple devices, but the cooperation of capricious mice is required, and examiners often have difficulty obtaining stable data. In contrast, using the present method, a mouse simply needs to be placed in the SCANET box, so that the acquisition of data is extremely easy.

5. Conclusion

In the evaluation of locomotor function in SCI model mice, inspections from various perspectives are desirable. Evaluation of maximum speed and acceleration of mouse movement with a SCANET system is simple, objective, and ethical. It is a novel and fine method for spinal cord-injured model mice and can complement other existing tests. Further examinations will be required for other animals.

Acknowledgments

The authors are grateful to Ms. Harada for the special care of the mice and to Drs. Nori and Yasuda for their excellent technical assistance during the surgical operations and data collection. This work was supported by the Project for Realization of Regenerative Medicine and Support for the core institutes for iPS cell research from the Ministry of Education, Culture, Sports, Science and Technology of Japan (MEXT).

References

[1] D. M. Basso, M. S. Beattie, and J. C. Bresnahan, "A sensitive and reliable locomotor rating scale for open field testing in rats," *Journal of Neurotrauma*, vol. 12, no. 1, pp. 1–21, 1995.

[2] D. M. Basso, L. C. Fisher, A. J. Anderson, L. B. Jakeman, D. M. McTigue, and P. G. Popovich, "Basso mouse scale for locomotion detects differences in recovery after spinal cord injury in five common mouse strains," *Journal of Neurotrauma*, vol. 23, no. 5, pp. 635–659, 2006.

[3] J. E. Beare, J. R. Morehouse, W. H. Devries et al., "Gait analysis in normal and spinal contused mice using the treadscan system," *Journal of Neurotrauma*, vol. 26, no. 11, pp. 2045–2056, 2009.

[4] M. Bervar, "Video analysis of standing—an alternative footprint analysis to assess functional loss following injury to the rat sciatic nerve," *Journal of Neuroscience Methods*, vol. 102, no. 2, pp. 109–116, 2000.

[5] L. de Medinaceli, W. J. Freed, and R. J. Wyatt, "An index of the functional condition of rat sciatic nerve based on measurements made from walking tracks," *Experimental Neurology*, vol. 77, no. 3, pp. 634–643, 1982.

[6] M. G. Fehlings, C. H. Tator, R. D. Linden, and I. R. Piper, "Motor and somatosensory evoked potentials recorded from the rat," *Electroencephalography and Clinical Neurophysiology*, vol. 69, no. 1, pp. 65–78, 1988.

[7] L. B. Goldstein and J. N. Davis, "Beam-walking in rats: studies towards developing an animal model of functional recovery after brain injury," *Journal of Neuroscience Methods*, vol. 31, no. 2, pp. 101–107, 1990.

[8] J. S. Soblosky, L. L. Colgin, D. Chorney-Lane, J. F. Davidson, and M. E. Carey, "Ladder beam and camera video recording system for evaluating forelimb and hindlimb deficits after sensorimotor cortex injury in rats," *Journal of Neuroscience Methods*, vol. 78, no. 1-2, pp. 75–83, 1997.

[9] Y. Mikami, M. Toda, M. Watanabe, M. Nakamura, Y. Toyama, and Y. Kawakami, "A simple and reliable behavioral analysis of locomotor function after spinal cord injury in mice: technical note," *Journal of Neurosurgery*, vol. 97, no. 1, pp. 142–147, 2002.

[10] W. B. J. Cafferty, N. J. Gardiner, P. Das, J. Qiu, S. B. McMahon, and S. W. N. Thompson, "Conditioning injury-induced spinal axon regeneration fails in interleukin-6 knock-out mice," *Journal of Neuroscience*, vol. 24, no. 18, pp. 4432–4443, 2004.

[11] Y. Mikami, H. Okano, M. Sakaguchi et al., "Implantation of dendritic cells in injured adult spinal cord results in activation of endogenous neural stem/progenitor cells leading to de novo

neurogenesis and functional recovery," *Journal of Neuroscience Research*, vol. 76, no. 4, pp. 453–465, 2004.

[12] K. Kawahats and M. Miyashita, "Electromyogram premotion silent period and tension development in human muscle," *Experimental Neurology*, vol. 82, no. 2, pp. 287–302, 1983.

[13] S. Rossignol, "Neural control of stereotypic limb movements," in *Handbook of Physiology*, L. B. Rowell and J. T. Sheperd, Eds., pp. 173–216, Oxford University Press, New York, NY, USA, 1996.

[14] H. Gee, "Animal guidelines," *Nature*, vol. 334, no. 6177, p. 7, 1988.

[15] A. S. Rivlin and C. H. Tator, "Objective clinical assessment of motor function after experimental spinal cord injury in the rat," *Journal of Neurosurgery*, vol. 47, no. 4, pp. 577–581, 1977.

21回日本末梢神経学会学術集会 特別講演

中枢神経系と末梢神経系の再生戦略*

岡野 栄之[1)], 辻 収彦[1),2)], 三浦 恭子[1),3)], 岡田 洋平[1)],
藤吉 兼浩[1),2)], 高木 岳彦[1),2)], 金子慎二郎[1),2)], 戸山 芳昭[2)],
山中 伸弥[3)], 中村 雅也[2)]

要旨 中枢神経系（脳と脊髄）は、再生が困難な臓器の代表例と考えられてきた。しかしながら、我々を含むいくつかのグループにより、ヒトを含めた哺乳類の成体の中枢神経系にも幹細胞が存在し、成体の脳内でニューロン新生が起きるとが示されてからこの状況は、大きく変わりつつある[1),2),3)]。中枢神経系の再生というと、① 神経軸索の再生、②疾患によって失われた細胞の補充、③機能回復という3つの側面を意味している[4)]。ここでは、中枢神経系を中心に、末梢神経系と比較しながら、両者の再生能力の違いを含め、再生医療に到る基礎研究・現状を紹介し、今後の展望について議論したい。

Key Words : Regeneration（再生）, Semaphorine（セマフォリン）, neural stem cell（神経幹細胞）, induced pluripotent stem cell (iPS cell)（人工多能性幹細胞）, transplantation（移植）

Peripheral Nerve 2010; 20(2): 145–151

1．神経軸索の再生

中枢神経系においては末梢神経系とは異なり軸索再生が起こりにくいということは、広く知られてきた事実である。近年、このよく知られた現象の裏には、実は軸索再生を阻害する中枢神経特有のメカニズムが存在することが明らかとなってきており、この阻害機構をターゲットとした研究が進んでおり、まさに軸索再生を目指した創薬研究のホットな題材となってきている。特に脊髄損傷における損傷部以下のレベルにおける麻痺は、神経軸索の断裂等に起因しており、損傷脊髄内での軸索再生の誘導が大きなテーマとなってきた。では、中枢神経系における軸索再生が何故難しいのか？この問題については、神経軸索の再生阻害活性を持つ膜蛋白が中枢神経系の髄鞘（ミエリン）に存在することが指摘されていたが、近年までその物質的な同定はなされていなかったのである。しかし現在では、中枢神経系における軸索再生阻害を担う分子の解明が進み、1. 中枢ミエリン由来タンパク質、2. グリア瘢痕由来の糖タンパク質、3. 線

Strategies for the regeneration of central and peripheral nervous systems.

[1)] Hideyuki OKANO, Osahiko TSUJI, Kyoko MIURA, Yohei OKADA and Kanehiro FUJIYOSHI：慶應義塾大学医学部生理学教室［〒160-8582 東京都新宿区信濃町35］：Departments of Physiology, School of Medicine, Keio University, Tokyo

[2)] Osahiko TSUJI, Kanehiro FUJIYOSHI, Takehiko TAKAGI, Shinjiro KANEKO, Yoshiaki TOYAMA and Masaya NAKAMURA：慶應義塾大学医学部整形外科学教室［〒160-8582 東京都新宿区信濃町35］：Departments of Orthopedic Surgery, School of Medicine, Keio University, Tokyo

[3)] Kyoko MIURA and Shinya YAMANAKA：京都大学iPS細胞研究所（CiRA）［〒606-8507 京都市左京区聖護院川原町53］：Center for Induced Pluripotent Stem Cell Research and Application, Kyoto University, Kyoto

維性瘢痕由来因子に大別されている[5]。

いくつかのグループにより、中枢神経系のミエリン形成細胞であるオリゴデンドロサイトの細胞膜に存在する再生阻害因子がNogoというligand分子として同定された。さらに、Nogoタンパク質の細胞外領域に対する結合するタンパク質分子としてNogo受容体が発見され、この受容体に結合するligand分子としてMAG、OMgpといったミエリン由来軸索再生阻害因子が次々と同定された現在ではオリゴデンドロサイトの細胞膜表面に存在するNogo、OMgp、MAGはニューロンに存在するNogo受容体に結合し、p75分子を共役分子として、細胞内へシグナルを伝え、低分子量タンパク質Rhoの活性化と、それに引き続くアクチン分子の重合阻害により、軸索突起の発芽や軸索再生を抑制するものと考えられている。注目すべきは、中枢ミエリン特異的なNogoやOMgpとは異なり、ＭＡＧは、中枢神経系のみならず、末梢神経系のミエリンの構成成分でもあり、末梢神経系の軸索の再生を制御する因子の一つといえよう[6]。

一方、グリア瘢痕に由来した細胞外基質であるコンドロイチン硫酸プロテオグリカン(chondroitin sulfate proteoglycan, CS-PG) が再生阻害タンパク質として重要である可能性が指摘されている。CS-PGは損傷周囲のグリア細胞から放出され、培養系でも軸索の伸展を阻害することが確認されている物質である。CS-PGによる再生阻害にはグルコサミノグリカン鎖による修飾が必要であることがわかっており、損傷部位にこのグルコサミノグリカン鎖を分解する酵素であるコンドロイチナーゼABCを投与することによって軸索の再生、運動機能の回復がみられたという報告がある[7]。我々の研究グループの池上らは、脊髄損傷モデルラットへ神経幹細胞移植とコンドロイチナーゼABCの併用により、単独使用群と比べてより大きな神経軸索再生効果が得られたことを明かにしている[8]。CS-PGの受容体分子は、長年謎であったが、最近の研究により、膜貫通型タンパク質脱リン酸化酵素であるPTPsigmaが、CS-PGの受容体であることが明らかになってきている。興味深いことに、PTPsigmaのノックアウトマウスにおいては、脊髄損傷後のCS-PG陽性のグリア瘢痕部分における軸索再生が誘導されることが明かになってきている[9]。

線維性瘢痕からは、セマフォリン、エフリンなどの軸索伸長阻害因子が供給されることもわかっており、われわれの研究グループにおいても、大日本住友製薬との共同により、新規のセマフォリン3A阻害剤xanthofulvinによる脊髄の軸索再生誘導と機能回復に成功している[10]。セマフォリン3Aは、Neuropilin-1分子を受容体としており、その共役受容体であるPlexin-Aや非受容体型チロシンキナーゼFynなどを介して軸索伸長阻害活性を示す。同セマフォリン3A阻害剤は、セマフォリン3Aに結合し、セマフォリン3AのNeuropilin-1分子への結合をブロックすることにより、その活性を示す。我々は、脊髄損傷モデル成体ラット（第8胸椎レベルでの完全切断モデル）へ上記のセマフォリン3A阻害剤を4週間に渡って投与し、損傷14週間後に解析したところ、同阻害剤投与群では対照群と比較して有意に神経軸索の再生が誘導されることを観察した。また同阻害剤投与により、神経軸索の再生以外に、損傷部に末梢神経系タイプのミエリン形成細胞であるシュワン細胞が移動し、再生したと思われる軸索に対してPoタンパク質陽性の末梢神経型のミエリンの形成が誘導されることを確認している。さらには、損傷部における細胞死を抑制したり、セマフォリン3AのNeuropilin-1分子への結合をブロックするため、血管誘導因子であるVEGFがおそらくNeuropilin-1分子との結合が促進されることにより血管新生などの種々の再生機転を促していることを明らかにした。次に、我々は同阻害剤投与群で、同上の脊髄損傷ラット（上記の完全切断モデル）の機能回復への効果

を検討した。対照群では、脊髄完全切断による後肢の完全麻痺は全く回復しなかったが、同阻害剤投与群では後肢の運動機能が有意に回復し、この回復が脳幹に起始し、脊髄を下降するセロトニン作動性ニューロン（縫線核脊髄路）の軸索再生によることを明らかにした。これらの報告を鑑みると、今後こういった分子の発現の誘導を制御し、軸索の伸展を許容する環境を作ることが、治療方法の開発において重要なテーマとなることは間違いない。

一方、このような齧歯類を用いた軸索再生の*in vivo*実験モデルには、限界があるのも事実である。第一の理由として、脊髄の構造と機能は、下行性線維の局在部位や局所の神経連絡など、種間、特に我々霊長類と齧歯類で著しく異なっている[11]。さらに、これまでの神経再生モデルでは、再生を誘導することが期待される薬剤や細胞移植を投与し、運動機能の回復などの観察により、十分効果が確認された後に、神経組織を固定し、標本を作製し、神経軸索の再生を組織化学的に確認することが解析法の主体であった。すなわち、動物の運動機能の回復と平行し、神経軸索の再生がどの程度起きているか？をリアル・タイム性を持って解析できていなかった。このような弱点を補うために我々は、小型霊長類であるマーモセットの脊髄損傷モデルを作成し、脊髄損傷における神経軸索の状況を可視化することを試みた[12]。現在の医療の場において、MRIは脊髄損傷患者の診断と治療の計画をたてるために必要不可欠である。われわれが作成したコモンマーモセットの脊髄損傷モデルにおいても、MRIが脊髄損傷後の組織の変化を反映していた。しかし従来のT1やT2強調像によって得られる脊髄の情報からは、白質と灰白質を明瞭に区別するのは困難である。従来のMRIは白質を均一な組織として描出するが、脊髄白質は実際には方向性を持った神経線維が複雑に配列している。長い間、生きたままの動物で白質の脊髄投射路を可視化する方法が求められていたが、近年、拡散テンソルトラクトグラフィー（Diffusion Tensor Tractography）（以下DTT）がこの能力を持つことが明らかとなった。拡散テンソルイメージング（拡散テンソルMRIと同義、以下DTI）によって得られたデータを解析し3次元に再構築することによってDTTが得られるが、DTTは例えば皮質脊髄路（Corticospinal Tract, ST）のような脳内の特定の神経投射路の走行を追跡することが可能である。しかし、依然としてDTTが解剖学的な軸索線維をどの程度反映しているのか、実際に組織と比較検討した報告はなかった。そこで我々は、コモンマーモセットの正常および損傷脊髄におけるDTTを行い、組織と比較することでDTTの精度と有用性を検証した。本研究では高分解能の画像を得るために7.0テスラーのMRIを用い、磁化率の影響を最小限にするためスピンエコー法を使用した。さらに、生体内の動きの影響を除去するため、まず最初に死後モデルを用いて解析を開始した。死後モデルを用いることで平均約10時間という長時間のMRI走査を行うことが可能となり、結果として高い空間分解能をもった画像を取得した。生きている動物を使った系では、すべての動物は全身麻酔を維持し,生体内の動きの影響を最小限にするために心臓（による影響）を制御した撮像方法を導入した。全身麻酔の下、マーモセットを特別に設計された頭部固定装置のついたアクリルベット上に固定した。麻酔上の問題により撮影時間は平均で1.5時間に抑えられ、そのために撮像範囲と空間分解能は死後モデルに比べて制限された。しかしDTTが生体内の神経経路を明らかにできる唯一の利用できる、発達した方法であるため、DTTが生きている動物の正常な投射路だけでなく途絶した投射路をも可視化したことは非常に重要なことである。

CSTは運動機能に関して最も重要な経路で

あり、しばしば脊髄損傷治療のプロトコールにおいて精査の対象になるため、本研究では特にCSTに焦点を絞って投射路選択的DTTを行ってきた。CST選択的DTTは実際に延髄から脊髄におけるCSTの走行を描出し、これまでDTTによる可視化は不可能と考えられてきた錐体交叉の描出をも可能とした。さらに脊髄半切モデルにおけるCST選択的DTTは、損傷部におけるCSTの途絶を明らかにした。

さらに我々は、DTT法によるイメージングを末梢神経の再生研究への応用を試みた。MRIは臨床の現場では欠かせないツールであるが、末梢神経の場合、周囲組織とのコントラストがつきにくいことから、その疾患の診断に適用されることはまれであり、理学所見や電気生理学的所見による侵襲的な補助診断に頼るのが現状である。これまでMRIによる末梢神経可視化の様々な試みがなされている。MR neurographyでは末梢神経を描出するように特別な撮像条件が設定されているが、定性的かつ主観的なものであり加えて神経線維の連続性を描出することは不可能であるため末梢神経再生を追跡することができない。神経線維を描出する他の方法としては超常磁性酸化鉄やガドリニウム製剤のような造影剤の注射であるが、侵襲を伴う。そのためこれらの方法では現在の臨床の現場で末梢神経損傷を評価するには困難である。これらの欠点を克服するため、DTT法に注目した。実験では、ラットの坐骨神経に圧挫損傷を加え、拡散テンソルイメージングから得られたデータを解析した[13]。このデータによって得られる画像であるDTTについては拡散異方性の指標であるfractional anisotropy（以下FA）値の閾値が0.4以上の異方性の強いところを任意の関心領域より追跡して描くと損傷神経の回復過程を明確に描出することが可能であった。損傷後早期では近位から描かれた線維は損傷部を越えて描かれないが、時間が経ち損傷部のFA値が回復してくると徐々に損傷部を越えて描けるようになり、損傷後3週で損傷前と同水準まで回復した。またこのDTTを描く指標となっているFA値と組織や機能評価の結果と比較した。末梢神経のFA値は髄鞘密度、髄鞘幅に比べ軸索密度、軸索径により強い相関を示した。この結果はこれまで報告されている軸索が髄鞘に比べ水分子の拡散異方性において重要な役割を果たしている仮説を支持するものであった。運動並びに機能評価についてはいずれも評価法においても損傷後1日に最も低下し、その後徐々に回復し6週には損傷前と同水準にまで回復した。これらの運動並びに知覚機能の回復は損傷部のFA値の回復と強い相関を示した。このように、組織学的、機能的変化とFA値との相関性が見出されたことで末梢神経のワーラー変性や再生に関わる種々の臨床的病態を評価するのに有用である可能性が示唆されるに至った。さらに今後の臨床応用に向けこの方法の有用性をみるため、生きたモデルにおけるさらに小さな神経を用いて撮像を試み、このトラクトグラフィーによって同一の動物で圧挫された神経の回復過程を描出することに成功した。以上より、末梢神経のDTTはその特性と限界を明確に理解した上で、末梢神経損傷の評価に革新的なツールとなることが示唆される。

2．細胞移植と細胞の補充

軸索再生の誘導に加えて、脊髄損傷の治療法として、脊髄損傷をきたす物理的なダメージ（一次損傷）に加えて、それに引き続く炎症・免疫学的反応などによる二次損傷によって失われたり、損傷を受けたニューロンやグリア、さらには血管系などを修復・補充するためには、幹細胞移植が期待されている[14]。これまで私達は、既存の齧歯類の脊髄損傷モデルに加え、マーモセットを用いた霊長類の脊髄損傷モデル（C5レベルの圧座損傷モデル）を独自に開発し[15]、細胞移植をはじめとするいくつかの治療手段の有効性を検証して

きた[16]。移植する細胞は、胎児由来神経幹・前駆細胞、ES細胞由来神経幹・前駆細胞、iPS細胞（後術）由来神経幹・前駆細胞、神経堤幹細胞などを検討してきた。例えば、この霊長類脊髄損傷モデルを活用し、ヒト胎児由来神経幹・前駆細胞移植を損傷後9日目に行った。2ヶ月後、移植したヒト胎児由来神経幹・前駆細胞は損傷部周囲に生着し、さらに頭尾側に移動し、ニューロン、オリゴデンドロサイト、アストロサイトへと分化していることを確認した[16]。運動機能評価においても移植群では非移植群と比較して有意な3次元自発運動量と上肢筋力の改善が得られた。脊髄損傷動物に対する神経幹細胞移植による機能回復のメカニズムとしては、解析していくと単に細胞補充だけではなく、次の3つの効果が考えられる。

①移植した神経幹・前駆細胞由来の介在ニューロンによる損傷脊髄内の局所神経回路網の部分的な修復、

②移植した神経幹・前駆細胞由来の幼弱なアストロサイトが産生する神経栄養因子・サイトカイン・細胞増殖因子や細胞外マトリックスによる細胞非自律的な栄養効果（宿主神経軸索の再生誘導、血管新生誘導）、

③移植した神経幹・前駆細胞由来のオリゴデンドロサイトによる宿主神経軸索の再髄鞘化

この研究結果は、将来における神経幹細胞移植の臨床応用の実現に向けた大きな前進と考えられた。しかし、我が国の「ヒト幹細胞を用いた臨床研究指針」（2006年施行）では、改正（2010年）後も、胎児由来の体性幹細胞は対象外であり、モラトリアム状態もしくは事実上の禁止状態が続いる。一方米国では、ステムセル社（StemCells, Inc.）によるpalmitoyl protein thioesterase-1（PPT1）というライソゾーム酵素欠損症（Batten病）に対する、胎児由来ヒト神経幹細胞（HuCNS-SC細胞）移植の臨床試験が進んでいる（第Ⅰ相終了）[17]。

我が国では、現時点では、ES細胞も「ヒト幹細胞を用いた臨床研究指針」の対象外であり、倫理的なハードルの低い成体組織由来の神経系の前駆細胞を用いた細胞移植治療の開発に、我々も集中することに方針を変更した。成体組織由来の神経系の前駆細胞のソースは、前述したiPS細胞（人工多能性幹細胞）由来神経幹・前駆細胞、神経堤幹細胞[18]などが期待できる。

皮膚などの体細胞にOct4, Sox2, Klf4, c-Mycといった少数の転写因子の遺伝子導入を行い、核情報のリプログラミングの結果を誘導した結果、ES細胞に類似した多能性幹細胞、すなわちiPS細胞が得られることが2006年に示された[19]。iPS細胞技術を用いることにより、ES細胞使用に伴う免疫拒絶や倫理的な問題が回避されると考えられ、将来の再生医療への応用が期待されている。2006年の秋には、iPS細胞の脊髄損傷への応用に向け慶應義塾大学と京都大学との共同研究チームが発足した。起源細胞や樹立法の異なる計36種類のマウスiPS細胞株を用い、これらをマウスES細胞で我々が構築してきた分化系を用いて神経幹・前駆細胞への分化誘導を行った。誘導された神経幹・前駆細胞を免疫不全マウス脳へ移植した解析から、神経幹・前駆細胞細胞集団中に未分化な細胞が残存しいる場合は移植によりテラトーマが発生し、iPS細胞由来神経幹・前駆細胞（ニューロスフェア）の腫瘍源性（テラトーマ形成の危険性）は、iPS細胞樹立時の起源細胞に依存していることが明らかとなった[20]。次に安全性についての厳格な評価により、すなわちiPS細胞由来の神経幹・前駆細胞集団中に分化抵抗性の未分化細胞の含量が検出されず、iPS細胞由来の神経幹・前駆細胞移植によりテラトーマ形成の危険性が低いことが示された事により、安全性の担保されたiPS細胞株（38C2株）を同定した。同iPS細胞株から誘導された神経幹・前駆細胞移植の

脊髄損傷への治療効果が証明された[21]。また、成体線維芽細胞より樹立されたiPS細胞由来の神経幹・前駆細胞の損傷脊髄への移植により、安全なiPS細胞株とそうでない細胞株の差が明瞭となった。このことは、iPS細胞を用いた再生医療において安全な細胞株を前もって準備するという他家移植の重要性を示唆している。運動機能の回復のメカニズムは、前出の神経幹細胞移植とほぼ同様のメカニズム（①～③）によるものと考えられる。現在、我々はヒトiPS細胞由来の神経幹細胞を用いた脊髄損傷モデルへの移植実験を進めている。

3．機能回復

機能的な再生は、患者さんのQOLを考えると、治療上最も重要なものとなり、必然的に再生医療の一環としての機能再生を目指したリハビリテーション医学が必須のものとなってくる[21]。上記の1．神経軸索の誘導、2．細胞移植と細胞補充のいずれもが、発生現象の再現を狙ったものであるが、発生過程では、シナプス形成を含むいろいろなイベントが、でたらめとまで言わないが比較的大雑把に進行し、その後神経系の機能成熟に伴い、activity-dependentに精細なものに集約していくことが知られている[22]。おそらく、中枢神経系の再生医療の過程に起きる機能再生過程においても同様なことが起きているものと予想出来る。従って、この観点からも、再生医療に伴う機能再生を増強するためにもリハビリテーションの効果が期待されている。現在臨床の現場で行われている亜急性および慢性期の脊髄損傷の患者さんを対象としたリハビリテーション療法として、体重を支えるトレッドミル・トレーニングによる歩行訓練や非麻痺側上肢抑制療法（麻痺側の上肢の強制使用）などが行われているが、これもこのような効果を狙ったものと考えられる。しかしその一方、臨床応用が始まっているとは言え、これらの治療法の神経メカニズムの解明には、やはり再生医学的あるいは神経科学的な観点からの動物実験を用いた検討が必須のものなる。メカニズムが解明されると、それが更に治療法の改善にもつながるであろう。この観点から、私達も、前出のセマフォリン3A阻害剤とリハビリテーションの併用によるラットの脊髄損傷の実験的治療を行っている。今後、さらに再生医療の治療効果を引き出すためにも、霊長類脊髄損傷モデルとBrain Machine Interface（BMI）を用いた次世代のリハビリテーションと再生医療の併用についても検討を行いたいと考える。これらの集学的な検討が、よりよい神経系の再生医療の開発につながるものと確信する。

文　献

1) Roy NS, Wang S, Jiang L, *et al.* In vitro neurogenesis by progenitor cells isolated from the adult human hippocampus. *Nat Med* 2000; 6: 271-277.
2) Okano H, Sawamoto K: *Philos Trans R Soc Lond B Biol Sci* 2008; 363: 2111-21122.
3) Okano H. Neural stem cells and strategies for the regeneration of the central nervous system. *Proc Jpn Acad, Ser* B 2010; 86: 438-450.
4) Okano H. Making and repairing the mammalian brain: Introduction. *Semin Cell Dev Biol* 2003; 14: 159.
5) Okano H, Kaneko S, Okada S, Iwanami A, Nakamura M, Toyama Y. Regeneration-based therapies for spinal cord injuries. *Neurochem Int* 2007; 85: 2332-2342.
6) Shen YJ, DeBellard ME, Salzer JL *et al.* Myelin-associated glycoprotein in myelin and expressed by Schwann cells inhibits axonal regeneration and branching. *Mol Cell Neurosci* 1998; 12: 79-91.
7) Bradbury EJ, Moon LD, Popat RJ *et al.* Chondroitinase ABC promotes functional recovery after spinal cord injury. *Nature* 2002; 416: 636–640.
8) Ikegami T, Nakamura M, Yamane J *et al.*

Chondroitinase ABC combined with neural stem/progenitor cell transplantation enhances their migration and axonal regeneration after rat spinal cord injury. *Eur J Neurosci* 2005; 22: 3036-3046.

9) Shen Y, Tenney AP, Busch SA *et al.* PTPsigma is a receptor for chondroitin sulfate proteoglycan, an inhibitor of neural regeneration. *Science* 2009; 326: 592-596.

10) Kaneko S, Iwanami A, Nakamura M *et al.*, A selective Sema3A-inhibitor enhances regenerative responses and functional recovery of the injured spinal cord. *Nat Med* 2006; 12: 1380-1389.

11) Lemon RN. Descending pathways in motor control. *Annu Rev Neurosci* 2008; 31: 195-218.

12) Fujiyoshi K, Yamada M, Nakamura M *et al.* In Vivo tracing of neural tracts in the intact and injured spinal cord of marmosets by diffusion tensor tractography. *J Neurosci* 2007; 27: 11991-11998.

13) Takagi T, Nakamura M, Yamada M *et al.* Visualizing for peripheral nerve degeneration & regeneration: Monitoring with diffusion tensor tractography. *NeuroImage* 2009; 44: 884-892.

14) Ogawa D, Okada Y, Nakamura M *et al.* Evaluation of human fetal neural stem/progenitor cells as a source for cell replacement therapy for neurological disorders: properties and tumorigenicity after long-term in vitro maintenance. *J Neuroci Res* 2009; 87: 307-317.

15) Iwanami A, Yamane J, Katoh H *et al.* Establishment of Graded Spinal Cord Injury Model in a Non-human Primate: the Common Marmoset. *J Neurosci Res* 2005; 80: 172-181.

16) Iwanami, A., Kakneko, S., Nakamura, M. *et al.* Transplantation of human neural stem/progenitor cells promotes functional recovery after spinal cord injury in common marmoset. *J Neurosci Res* 2005; 80: 182-190.

17) Tamaki SJ, Jacobs Y, Dohse M *et al.* Neuroprotection of host cells by human central nervous system stem cells in a mouse model of infantile neuronal ceroid lipofuscinosis. *Cell Stem Cell* 2009; 5: 310-319.

18) Nagoshi N, Shibata S, Kubota Y *et al.* Ontogeny and Multipotency of Neural Crest-Derived Stem Cells in Bone Marrow, Dorsal Root Ganglia and Whisker Pad of Adult Rodents. *Cell Stem Cell* 2008; 2: 392-403.

19) Takahashi, K., Yamanaka, S. Induction of pluripotent stem cells from mouse embryonic and adult fibroblast cultures by defined factors. *Cell* 2006; 126: 663-676.

20) Miura K, Okada Y, Aoi T. *et al.*, Variation in the safety of induced pluripotent stem cell lines. *Nature Biotechnol* 2009; 27: 743-745.

21) Tsuji O, Miura K, Okada Y *et al.* Therapeutic effect of the appropriatelly evaluated 'safe' iPS cells for spinal cord injury. *Proc. Natl. Acad. Sci. USA* 2010; 107: 12704-12709.

22) 岡野　栄之：幹細胞医学の進展と中枢神経系の再生戦略. *あいみっく* 2010; 31: 3-6.

23) Goodman CS, Shatz CJ. Developmental mechanisms that generate precise patterns of neuronal connectivity. *Cell* 1993; 72: Suppl: 77-98.

第1章：画像検査法編

2．脊椎脊髄における画像診断技術の最近の進歩

拡散テンソル tractography*

藤吉　兼浩**　辻　収彦　松本　守雄
千葉　一裕　戸山　芳昭　中村　雅也

はじめに

白質神経線維など，方向性を有する生体構造に生じる水分子の制限された拡散に着目し，その拡散異方性をとらえようとする磁気共鳴像を拡散テンソル MRI または拡散テンソルイメージング（diffusion tensor imaging：DTI）と呼ぶ．さらに，拡散異方性の最大方向を追跡することにより得た画像を拡散テンソル tractography（diffusion tensor（fiber）tractography：DTT）という．最近では脊髄領域における DTT の報告も多くなってきている．本稿では DTT の基本的原理を概説するとともに，脊髄における DTT の特徴について述べることにする．

拡散 MRI と異方性

脊椎脊髄領域における核磁気共鳴像（MRI）の有用性については異論の余地はないが，最近は拡散 MRI（diffusion MRI）という言葉も広く認知されてきた．脳における拡散 MRI の報告は 1980 年代からはじまり[11,12]，1990 年代の急性期脳梗塞における有用性の報告によって世界中で知られることとなった[3,4]．最近では悪性腫瘍の転移を 3 次元的に評価し得る diffusion weighted whole body imaging with background body signal suppression（DWIBS）の出現によってますますその有用性が期待されている[24]．拡散とは“水分子の拡散”のことであり，これを利用した MRI 全般を拡散 MRI という．ここでいう拡散は水分子の Brown 運動を意味し，水分子の流れ（flow）とは厳密に区別される．Motion proving gradient（MPG）と呼ばれる傾斜磁場を付加することで，組織内の水分子の拡散情報を検出・可視化したものが拡散強調像（diffusion weighted MR imaging：DWI[注1)]）であり，われわれ臨床医が通常目にするのはこの DWI である．DWI は既存の MRI の撮像方法とは異なり，拡散に基づいたコントラストが多くの病変において新たな情報をもたらす．

生体組織では，水分子の拡散の方向は多かれ少なかれ制限を受ける．方向によって拡散の速度が

Key words
脊髄（spinal cord）
拡散テンソル tractography
（diffusion tensor tractography）
MRI

注1) DWI は教科書では“プロトンの拡散運動をなんらかの方法で強調した MRI すべてを含むが，通常は狭義の使い方として拡散強調の傾斜磁場を加えて撮像した元画像をさす”とある[1]．

* Diffusion Tensor Tractography

** 慶應義塾大学医学部整形外科〔〒160-8582 新宿区信濃町 35〕／Kanehiro FUJIYOSHI, Osahiko TSUJI, Morio MATSUMOTO, Kazuhiro CHIBA, Yoshiaki TOYAMA, Masaya NAKAMURA：Department of Orthopaedic Surgery, School of Medicine, Keio University

0914-4412/10/¥400/論文/JCOPY

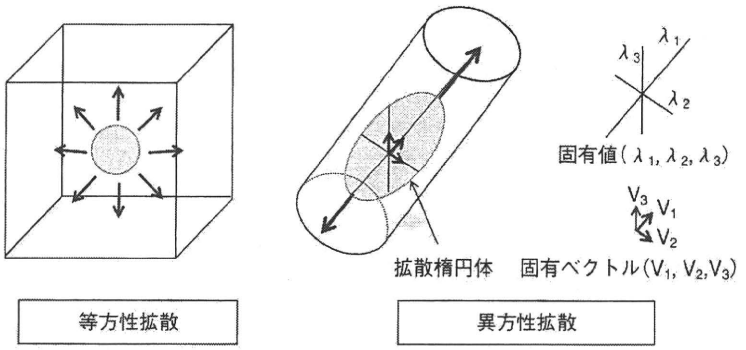

図 1　水分子の拡散
水分子の拡散は，球形で表される等方性拡散と，楕円体で表される異方性拡散の2つに分けられる．各ボクセルにおける異方性は拡散楕円体に近似される．

異なる性質のことを拡散の異方性または異方性拡散（anisotropic diffusion）と呼ぶが[13]，病巣の検出を目的とするDWIでは正常な白質の信号値が変化するのを避けるため，あえて異方性が少なくなるような撮像法あるいは処理を行っている．このため異方性拡散の影響を排除した拡散強調像を，等方性拡散強調像（isotropic diffusion-weighted image：isotropic DWI）と呼ぶこともある．異方性拡散は楕円体で表され，等方性拡散は球体で表される（図 1）．

脊髄白質は頭尾側方向に比較的整然と走行する神経線維束からなり，その中の水は構成要素である軸索の走行に沿って拡散する．このため白質は拡散異方性が大きい．この異方性の情報から神経線維を追跡・可視化したものがDTTである．DTTを構築するためには拡散の大きさ表す見かけの拡散係数（apparent diffusion coefficient：ADC）や，拡散の異方性を表すfractional anisotropy（FA）などのパラメーターを求める必要がある．これらのパラメーターを求める過程でテンソル解析を用いるが[2,14,17]，これが拡散テンソルの名前の由来である[注2)]．

異方性の計測とテンソル解析

1 FAとFAマップ

異方性の計測にはいろいろな方向における拡散の情報が必要であるため，最低6軸以上でMPGを付加したMRIと，MPGを付加しないT2強調像を撮像する必要がある．これによって得られたデータをテンソル解析することで，拡散の大きさを決定する固有値（λ_1, λ_2, λ_3）と方向を決定する固有ベクトル（v_1, v_2, v_3）が算出される．これらの値から各ボクセルにおける異方性の情報は楕円体として近似されるが，これを拡散楕円体という（図 1）．この情報を2次元で描出したものをFAマップ（または異方性マップ）という（図 2）．FAとは異方性の大きさの指標として用いられ，0から1の値をとるが，等方性拡散においては0となり，異方性が大きくなるほど1に近づく．FAに対し，ADCは拡散の方向とは無関係に拡散の大きさを表す指標である．FAは以下の式により算出される．

$$ADC=\frac{\lambda_1+\lambda_2+\lambda_3}{3}=\langle D\rangle$$

$$FA=\sqrt{\frac{3}{2}}\frac{\sqrt{(\lambda_1-\langle D\rangle)^2+(\lambda_2-\langle D\rangle)^2+(\lambda_3-\langle D\rangle)^2}}{\sqrt{\lambda_1^2+\lambda_2^2+\lambda_3^2}}$$

注2)　テンソルとは多線形性をもつベクトル変数の関数であり，ベクトルに（左から）かけるとベクトルを生むような行列で，行列の各成分が座標系と密接に関連しているものである[13]．実際には3×3，2階の行列演算が必要である．